Low Temperature Physics/Fizika Nizkikh Temperatur, 2013, v. 39, No. 4, pp. 452–458

Grain size effect on magnetic properties of $REMnO_3$ (RE = Pr, Nd)

V. Dyakonov[1,2], W. Bażela[3], R. Duraj[3], M. Dul[3], Z. Kravchenko[2], E. Zubov[2], K. Dyakonov[4], S. Baran[5], A. Szytuła[5], and H. Szymczak[1]

[1]*Institute of Physics, PAS, 32/46 Al. Lotników, Warszawa 02-68, Poland*

[2]*A.A. Galkin Donetsk Physico-Technical Institute, National Academy of Sciences of Ukraine*
72 R. Luxembourg Str., Donetsk 83114, Ukraine
E-mail: zubov@fti.dn.ua

[3]*Institute of Physics, Technical University, 1 Podchorążych, Kraków 30-084, Poland*

[4]*A.F. Ioffe Physico-Technical Institute RAN, 26 Politekhnicheskaja, St.-Petersburg 194021, Russia*

[5]*M. Smoluchowski Institute of Physics, Jagiellonian University, 4 Reymonta, Kraków 30-059, Poland*

Received September 25, 2012

X-ray diffraction and magnetic using dc and ac methods measurements of the polycrystalline and nanosize $REMnO_3$ (RE = Pr, Nd) powdered samples have been performed. The nanosize manganites were synthesized with a sol-gel method at different (800, 850 and 900 °C) temperatures. The average size of synthesized nanoparticles (from 56 to 89 nm) and polycrystalline powders (above 200 nm) was estimated using the x-ray diffraction data. All the compounds studied crystallize in the orthorhombic crystal structure (space group *Pnma*) at room temperature with smaller values of the lattice parameters in the nanosamples. The temperature-dependent ac magnetic susceptibilities show a sharp high-temperature peak connected with Mn magnetic moments ordering. The low-temperature maximum of magnetic susceptibility is proposed to be due to the polarization of the rare-earth sublattice by an effective exchange field of the Mn ordered sublattice. The antiferromagnetic ordering of Mn sublattice and paramagnetic Curie temperatures as well as the magnetic moment values for the nanosize samples were found to be smaller than those for polycrystalline sample.

PACS: **75.30.–m** Intrinsic properties of magnetically ordered materials;
75.60.–d Domain effects, magnetization curves, and hysteresis;
75.75.–c Magnetic properties of nanostructures.

Keywords: x-ray diffraction, magnetic ordering, exchange interactions, nanoparticle, sol-gel method.

1. Introduction

$REMnO_3$ (RE are the rare-earth ions) manganites have been the subject of intensive investigations which are concentrated on their magnetic and electronic properties. In the $REMnO_3$ series, an increase of the Néel temperature with increasing number of Z for the rare-earth elements is observed. The fundamental interest in these compounds is the explanation of the complex magnetic interactions and correlation of the magnetic, structural and electronic properties in these compounds [1].

The results of studies of crystal and magnetic properties of $REMnO_3$ manganites, where RE = Pr and Nd, are reported in the number works [2–8]. These compounds crystallize in the orthorhombic crystal structure described by the *Pnma* space group. Neutron powder diffraction (NPD) data indicate that both compounds are antiferromagnets with the Néel temperatures equal to 86 K for $PrMnO_3$ [2] and 78 K for $NdMnO_3$ [3] below which the magnetic moments of the Mn atoms order. In contradiction, the specific heat and thermal expansion data for $PrMnO_3$ and $NdMnO_3$ single crystals [4,5] indicate the anomalies connected with the ordering in Mn sublattice at 99 and 88 K, respectively. It is also proposed that below 13 K in $PrMnO_3$ and below 18 K in $NdMnO_3$ the magnetic moments of rare-earth elements order [4,6]. In the $PrMnO_3$ single crystal, the Mn moments is established to form the canted structure described by C_xF_y arrangement whereas Pr moments form

the ferromagnetic structure of the F_y-type [2]. Similar magnetic structures are observed in the $NdMnO_3$ single crystal [3].

The ground state of the rare-earth ions in the $PrMnO_3$ and $NdMnO_3$ single crystals was studied in Ref. 6. Electron transitions inside of both the ground Pr^{3+} quasidoublet split by a crystal field and Nd^{3+} Kramers doublet split by exchange Mn–Nd field were revealed and their crystal field and exchange splitting components were determined.

Physical properties of manganites are known to depend on various factors including stoichiometry and grain size. A main motivation for performed studies was to obtain the data concerning the crystal structure and magnetic properties of $REMnO_3$ (RE = Pr, Nd) manganites as a function of the grain size.

In this work, in order to understand the magnetic phenomena in nanopowdered manganites and to compare obtained data with data for polycrystalline powders the detailed studies of $PrMnO_3$ and $NdMnO_3$ have been carried out. Magnetic data demonstrate the large difference between the magnetic ordering of poly- and nanopowders. The nanosamples are characterized by smaller values of both the Néel temperature and the paramagnetic Curie temperature. The magnetic moment values for the nanosize samples are also smaller than for polycrystalline sample.

2. Experiment

The bulk polycrystalline $NdMnO_3$ and $PrMnO_3$ samples were prepared using the standard solid-state reaction technique described in Refs. 7, 8. In brief, the mixture of high-purity praseodymium (Pr_2O_3) or neodymium (Nd_2O_3) oxides and manganese oxide (Mn_3O_4) taken in stoichiometric ratio was dissolved in diluted (1:1) nitric acid. The obtained solution was evaporated to a complete removal of water followed by a degrading of nitrite salts at 500–700 °C. The product obtained was grinded and then was heated to 900–950 °C for 2 h to remove a salt-disintegration products. The homogeneous powder compacted under pressure of 1 GPa into pellets were sintered in air at 1150–1170 °C for 18–20 h followed by temperature decrease to the room temperature at the rate of 70 °C/h. Because of high temperatures of synthesis the grain sizes of polycrystalline samples has exceeded nanosizes.

The nanoparticle $PrMnO_3$ and $NdMnO_3$ manganites were prepared using the sol-gel method. To prepare nanopowder $PrMnO_3$, a stoichiometric amount of Pr_6O_{11} and Mn_3O_4 oxides of high purity was dissolved in acetic acid with added hydrogen peroxide. An urea as a gel-forming component was added to the solution obtained. This mixture was slowly evaporated to dryness. The dry remainder was decomposed with smoothly increasing temperature from 200 to 450 °C. Then the powder obtained was thoroughly grinded. The pressed pellets were annealed at temperatures of T_{an} = 800 and 900 °C for 20 h in air followed by a slow cooling down to the room temperature.

For synthesis of the nanoparticle $NdMnO_3$ manganites, a stoichiometric amount of the Nd_2O_3 and Mn_3O_4 oxides of high purity were used. Neodymium oxide was dissolved (1:1) in a dilute nitric acid, and Mn_3O_4 oxide was dissolved in acetic acid with added hydrogen peroxide. Both solutions were mixed together with added solution of urea. This mixture was slowly evaporated to dryness. The dry remainder was calcinated at temperature of 200–450 °C. Then the dry powder obtained was grinded and was pressed into pellets which were annealed at T_{an} = 800, 850 and 900 °C for 20 h in air followed by a slow cooling down to the room temperature.

In order to determinate the crystallographic structure all the samples studied were characterized at room temperature with x-ray powder diffraction using a Philips PW-3710 X'PERT diffractometer with CuK_α radiation. The 2θ scans are performed with the steps of 0.01 and counting time of 5 s step. The data were analyzed with the Rietveld-type refinement software FullProf program [9]. Magnetization and magnetic susceptibility of both nanoparticles and polycrystalline samples have been measured using a vibrating sample magnetometer option of the Quantum Design PPMS over a temperature range 1.9–300 K in magnetic field up to 90 kOe. The following measurements have been performed:

— temperature dependence of dc magnetic ZFC (zero field cooling) and FC (field cooling) susceptibilities (χ_{dc}) in magnetic field of 50 Oe (to determine the phase transition temperature);

— $\chi_{dc}(T)$ dependence in temperature range of 1.9–300 K in magnetic field of 1 kOe (to determine the paramagnetic Curie temperature, θ_p, and the effective magnetic moment value, μ_{eff});

— field dependence of magnetization in magnetic field up to 90 kOe (to determine the magnetic moment values).

The ac magnetic susceptibility, $\chi_{ac} = \chi' + \chi''$, where χ' and χ'' are the real and imaginary components, respectively, was also measured versus temperature and frequency between 10 Hz and 10 kHz in magnetic field with H_{ac} amplitude equal to 5 Oe.

3. Results

Typical x-ray pattern for nano-$PrMnO_3$ (T_{an} = 800 °C) is presented in Fig. 1. The x-ray diffraction data indicate that all the samples studied are homogeneous, single phase and have an orthorhombic crystal structure described by the *Pnma* space group. In this structure the Pr or Nd and O1 atoms occupying the 4(*c*) site: *x*, ¼, *z*; Mn atoms in 4(*b*) site: 0, 0, ½; and O2 atoms in the 8(*d*) site: *x*, *y*, *z*. The fitted structural parameters: lattice *a, b* and *c* constants and unit cell volume, *V*, and positional x_i, y_i and z_i parameters are listed in Table 1. The decrease of the *a, c* constants and

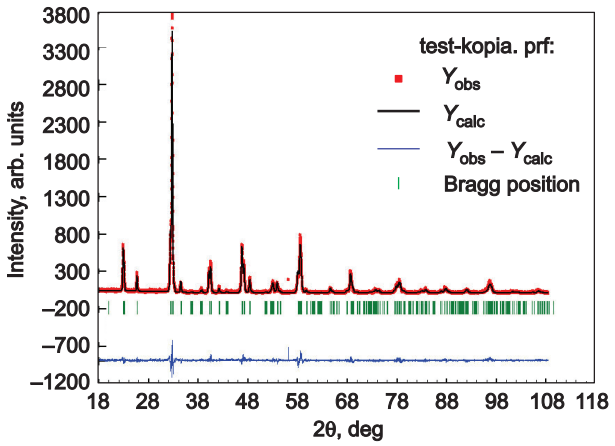

Fig. 1. X-ray diffraction pattern of nano-800 °C $PrMnO_3$ observed (solid squares) and calculated (solid lines). Bragg reflections are indicated by tick marks and the difference pattern is also plotted.

unit cell volume, V, and increase of the b constant were found with decreasing the grain size.

The grain sizes, d, in nanopowder were determined using the Scherrer relation of $d = \lambda/(B \cos\theta)$ [10]. Here $\lambda = 1.54178$ Å is the x-ray wavelength, θ the corresponding angle of Bragg diffraction and $B = \beta - \beta_0$ the difference between the Bragg reflex half-widths of the nanosize samples (β) and standard Si powder sample (β_0) with the grain size of 10 μm [11] which was used to calibrate the intrinsic width associated to the equipment. The singular (111) reflection of the diffraction pattern was used to calculate the particle size. The d values calculated are listed in Table 2. Presented data indicate that the grain sizes increase with increasing annealing temperature.

Table 2. The grain sizes, d, of $REMnO_3$ nano- and polycrystalline powders calculated using XRD data and the Scherrer relation

Sample		<d>, nm
$PrMnO_3$	800 °C	66
	900 °C	85
	poly	250
$NdMnO_3$	800 °C	56
	850 °C	70
	900 °C	89
	poly	245

Figiure 2(a)–(c) present the results of magnetic studies of the $PrMnO_3$ samples. The temperature dependences of dc magnetic susceptibility, $\chi_{dc}(T)$, for poly- and nanosamples are shown in Fig. 2(a). Presented data point to a distinct splitting between the dc susceptibilities measured under field-cooled (FC) and zero-field-cooled (ZFC) conditions. These curves are separated below the temperatures of 90 K for poly-, 65 K for nano-900 °C and 60 K for nano-800 °C samples. The ZFC curves have the maximum at 68, 45 and 35 K for poly-, nano-900 °C and nano-800 °C samples, respectively. Such behavior of $\chi_{dc}(T)$ seems to be connected with the freezing of the domain dynamics within the ordered Mn sublattice. The antiferromagnetic (AFM) phase transition temperature, T_N, defined as maximum of $d\chi_{dc}/dT$ dependence was found to decrease with decreasing the grain sizes (Table 3).

Above 150 K, the reciprocal magnetic susceptibilities (Fig. 2(b)) obey the Curie–Weiss (CW) law: $\chi_i = \chi_{0i} + C_i/(T - \theta_i)$, where C_i is the Curie–Weiss constant, χ_{0i} is the background susceptibility and θ_i is the Curie–Weiss temperature. The values of the paramagnetic

Table 1. Structural parameters for $NdMnO_3$ and $PrMnO_3$ obtained in the Rietveld refinement from x-ray patterns at room temperature

Parameter	$NdMnO_3$				$PrMnO_3$		
	poly	nano			poly	nano	
		900 °C	850 °C	800 °C		800 °C	900 °C
a, Å	5.7119(9)	5.6512(5)	5.6283(4)	5.6125(2)	5.6049(5)	5.5192(2)	5.5490(2)
b, Å	7.5890(13)	7.6117(7)	7.6199(6)	7.6234(2)	7.6654(7)	7.6995(3)	7.6908(3)
c, Å	5.4191(8)	5.4140(5)	5.4129(4)	5.4120(2)	5.4616(5)	5.4547(2)	5.4550(2)
V, Å^3	234.60(11)	232.88(7)	232.14(6)	231.56)2)	234.65(6)	231.80(2)	232.88(2)
RE x	0.0597(7)	0.0563(3)	0.0552(3)	0.0536(2)	0.0464(8)	0.0391(2)	0.0427(2)
z	0.9909(9)	0.9929(6)	0.9914(5)	0.9913(3)	0.9949(11)	0.9955(4)	0.9927(4)
O1 x	0.4837(8)	0.467(3)	0.467(3)	0.481(2)	0.4854(7)	0.493(2)	0.496(2)
z	0.0817(8)	0.103(4)	0.101(4)	0.090(2)	0.0760(7)	0.073(3)	0.074(3)
O2 x	0.3106(6)	0.294(3)	0.290(3)	0.302(1)	0.3013(4)	0.292(2)	0.287(2)
y	0.0405(4)	0.042(2)	0.040(2)	0.041(1)	0.0385(3)	0.034(1)	0.038(1)
z	0.7108(6)	0.725(3)	0.727(3)	0.713(2)	0.7169(4)	0.716(2)	0.721(2)
R_{Bragg}, %	6.8	8.4	13.8	9.0	7.8	5.2	6.6
R_f, %	4.4	7.4	8.8	9.8	6.4	6.6	7.1

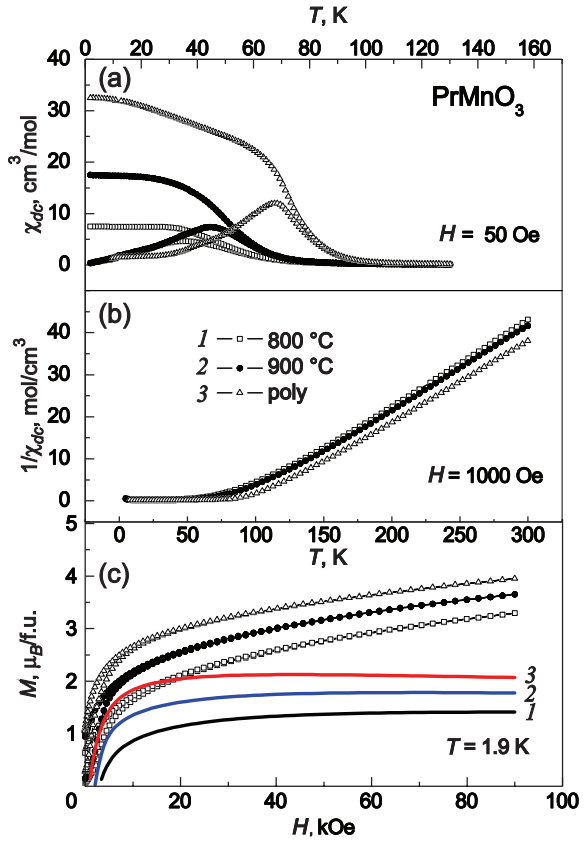

Fig. 2. $PrMnO_3$: (a) Temperature dependence of the dc magnetic susceptibility for poly- and nanosamples. Lower and upper curves correspond to ZFC and FC susceptibilities, respectively; (b) Temperature dependences of the reciprocal magnetic susceptibility; (c) Experimental field dependences (points) of magnetization of $PrMnO_3$ at 1.9 K for nano-800 °C (squares), nano-900 °C (circles) and poly (triangles). The solid lines *1–3* correspond to magnetization of nano-800 °C, nano-900 °C and poly without magnetic contribution of Pr^{3+} ions, respectively.

Curie temperature and effective magnetic moment are listed in Table 3.

The θ_p temperature for $PrMnO_3$ decreases from 104 K for poly- to 88 and 81 K for nano-900 °C and nano-800 °C samples, respectively. A shift of the CW temperature towards lower temperatures indicates a decrease of magnetic interactions between Mn moments with decreasing the grain size. A positive Curie–Weiss temperature despite the AFM transition can be understood considering the magnetic structure with ferromagnetic coupling in the plane and AFM coupling between planes.

The values of effective magnetic moments are compared with calculated values from the relation of

$$\mu_{\text{eff}} = \sqrt{(\mu_{\text{eff}}^{\text{RE}})^2 + (\mu_{\text{eff}}^{\text{Mn}})^2} \ , \qquad (1)$$

where $\mu_{\text{eff}}^{\text{Pr}} = 3.58\ \mu_B$ and $\mu_{\text{eff}}^{\text{Mn}} = 4.90\ \mu_B$ are the theoretical values for Pr^{3+} and Mn^{3+} ions, respectively.

The effective magnetic moments are larger than theoretical value $\mu_{\text{eff}} = 6.07\ \mu_B$. It can be connected with existence of ferromagnetic clusters which at high temperatures behave as the superparamagnetic particles having, as a rule, the large value of effective magnetic moment.

Magnetic field dependences of magnetization of $PrMnO_3$ are shown in Fig. 2(c). As it is seen in Fig. 2(c), the magnetic moments per formula unit are equal to 3.3 (nano-800 °C), 3.6 (nano-900 °C) and 3.9 μ_B (poly-) at T = = 1.9 K in magnetic field H = 90 kOe (Table 3). The magnetization increases as magnetic field is increased, without reaching the saturation. The lack of saturation at T = 1.9 K and H = 90 kOe is due to Mn antiferromagnetism.

Table 3. Magnetic data for $REMnO_3$ (RE = Pr and Nd) compounds

Compound	T_N, K	T_t, K	θ_p, K	μ_{eff}, μ_B	μ, μ_B	μ, μ_B, Mn^{3+}
$PrMnO_3$						
poly	74	10	104	6.5	3.9	2.1
nano-800 °C	50		81	6.4	3.3	1.4
nano-900 °C	56	15	88	6.4	3.6	1.7
$NdMnO_3$						
poly	70	11	68	6.2	4.2	2.0
nano-800 °C	50	7	58	6.1	3.7	1.7
nano-850 °C	55	9	62	6.1	3.8	1.8
nano-900 °C	55	10	67	6.2	4.0	1.9

Comments: T_N is the temperature of antiferromagnetic ordering of Mn sublattice determined as the $d\chi_{dc}/dT$ maximum; T_t is the temperature of rare-earth polarization; θ_p is the paramagnetic Curie temperature; μ_{eff} is the effective magnetic moment determined from the Curie–Weiss law; μ is the magnetic moment per formula unit determined from magnetization at T = 1.9 K and H = 90 kOe; μ, Mn^{3+} is the magnetic moment per formula unit of Mn^{3+} subsystem in applied magnetic field without contribution of Mn–Pr and Mn–Nd exchange interactions.

For polycrystalline $PrMnO_3$ samples, the temperature dependence of χ'_{ac} susceptibility shows the sharp maximum at 70 K and weak anomaly at 10 K (Fig. 3(a)), which correspond to two peaks in temperature dependence of χ''_{ac} susceptibility at the same temperatures. Their intensity decreases with increasing frequency.

For nano-900 °C, the $\chi'_{ac}(T)$ dependence exhibits the sharp maximum at 48 K and a slightly pronounced anomaly at 15 K, while the $\chi''_{ac}(T)$ dependence has two maxima at 46 and 13 K (Fig. 3(b)). The position and intensity of $\chi''_{ac}(T)$ maximum change with changing frequency.

For nano-800 °C, alone $\chi'_{ac}(T)$ maximum is observed at 41 K (Fig. 3(c)). Both an intensity and temperature of the $\chi''_{ac}(T)$ peak increase with increasing frequency.

For $NdMnO_3$ the temperature and magnetic field dependences of susceptibility and magnetization are analogous to those for $PrMnO_3$ shown in Figs. 2 and 3 (therefore they are not presented). They show the following:

— the temperature-dependent dc magnetic susceptibilities of $NdMnO_3$ resemble the results obtained for $PrMnO_3$. The ZFC and FC curves are observed to be separated at 74 K (for poly-) and 55 K (for nano-900 °C) and 50 K (for nano-800 and 850 °C);

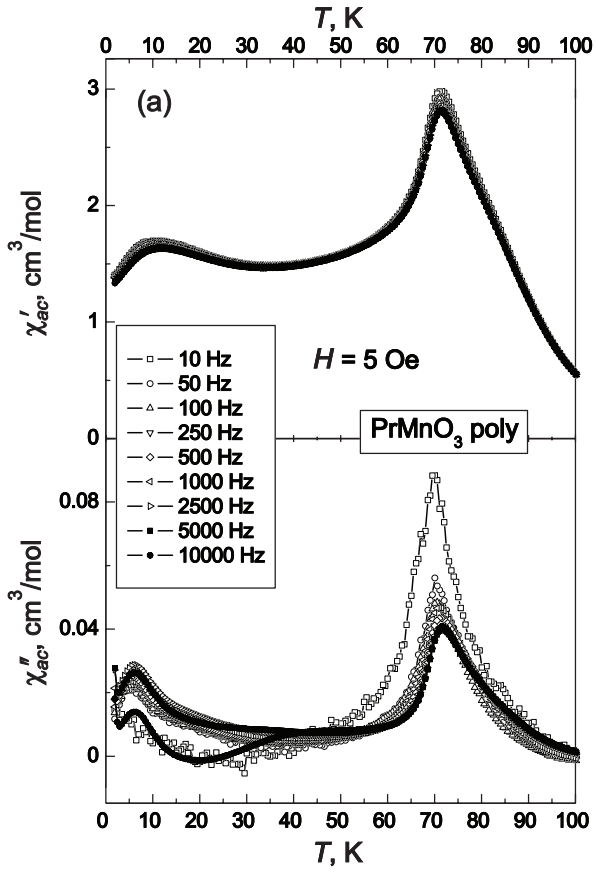

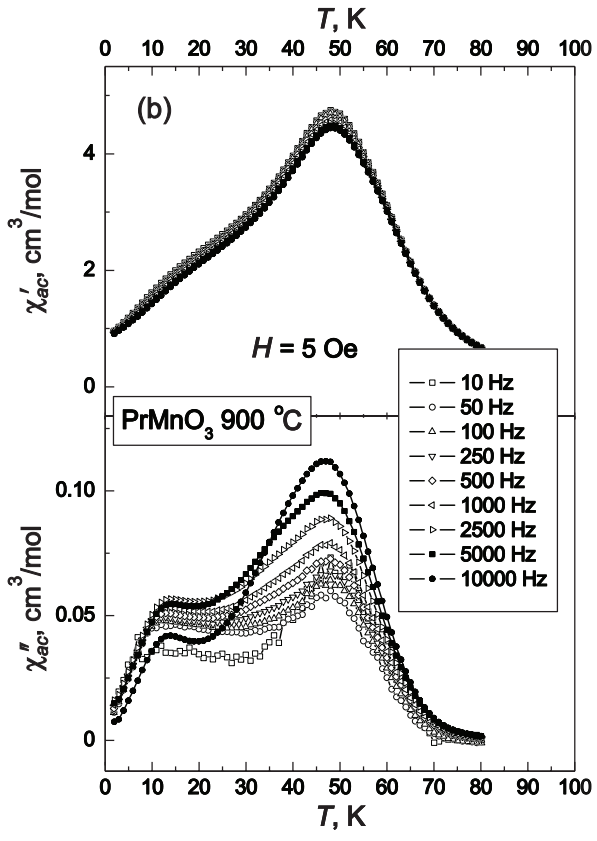

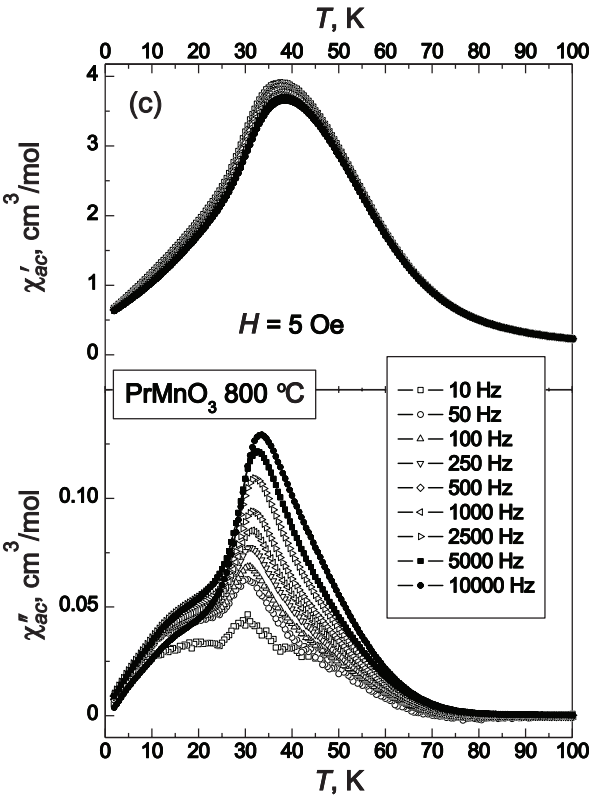

Fig. 3. Temperature dependences of the real χ'_{ac} and imaginary χ''_{ac} components of the ac magnetic susceptibility of the $PrMnO_3$ samples: (a) poly-, (b) nano-900 °C and (c) nano-800 °C measured in magnetic field of H = 5 Oe at the frequencies varied between 10 Hz and 10 kHz.

— the reciprocal magnetic susceptibility for poly- and nanosamples obeys the Curie–Weiss law at temperatures above the AFM phase transition. The paramagnetic Curie temperatures and the effective magnetic moments calculated are displayed in Table 3. The experimental data are close to the theoretical value of effective moment μ_{eff} = = 6.09 μ_B for the superposition of the Nd($4f^3$) and the Mn($3d^4$) sublattices;

— the total magnetic moments calculated are equal to 4.2, 4.03, 3.87 and 3.75 μ_B/f.u. for poly-, nano-900, nano-850 and nano-800 °C, respectively, at T = 1.9 K in magnetic field H = 90 kOe.

The temperature dependences of χ'_{ac} and χ''_{ac} components of ac susceptibility resemble the results obtained from dc measurements. For example, in Fig. 4 the $\chi_{ac}(T)$ dependences are presented for nano-800 °C $NdMnO_3$, which exhibit two sharply pronounced maxima. The temperature and intensity of both maximum are slightly dependent on frequency.

The characteristic peculiarity of the $\chi'_{ac}(T)$ susceptibility is related to an occurrence of a cusp at $T \approx 11$ K which is accompanied by a peak in the $\chi''_{ac}(T)$ susceptibility. It may be assumed (as in Ref. 6) that this low-temperature maximum is due to the polarization of the Nd sublattice by an effective exchange field of the Mn sublattice and obvi-

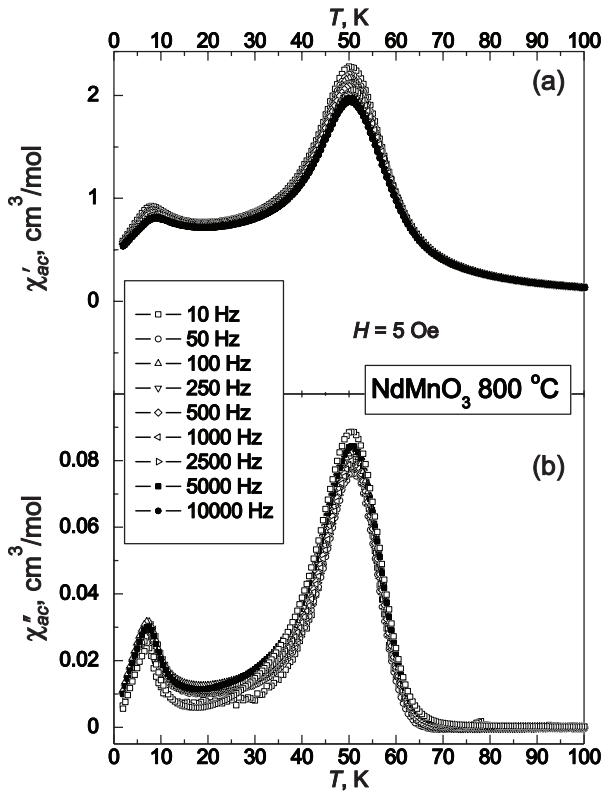

Fig. 4. Temperature and frequency dependences of the real χ'_{ac} (a) and imaginary χ''_{ac} (b) components of the ac magnetic susceptibility of the nano-800 °C $NdMnO_3$ sample.

ously results in the additional contribution of the Nd ions to a weak magnetic moment.

4. Discussion

To calculate the magnetic moment of $PrMnO_3$ in applied magnetic field it is necessary to take into account the contribution of the Pr^{3+} sublattice. As is shown in Ref. 4, for the $PrMnO_3$ single crystal the lowest level of Pr^{3+} is split in quasidoublet by crystal field and superexchange rare-earth ion with Mn^{3+} ion. The Δ value of this splitting can be written as

$$\Delta = 2\left[\Delta_{cf}^2 + \Delta_z^2 + (\boldsymbol{\mu}\mathbf{H})^2\right]^{1/2}, \qquad (2)$$

where $2\Delta_{cf}$ and $2\Delta_z$ are the splitting by the crystal field and Pr–Mn exchange interactions, respectively, and μ = = (μ_a, μ_b, 0) is the magnetic moment of ground state in *ab* plane. The Pr^{3+} contribution to Δ is caused by both Δ_{cf} = = 18.7 K [4] and energy of interaction of μ magnetic moment with applied field. One can write the next expressions for magnetic moment per formula unit along the $x = a$, b and $z = c$ directions [4]:

$$M_x = \frac{2\mu_x^2 H_x}{\Delta}\tanh\left(\frac{\Delta}{2k_BT}\right) + \chi_x^{VV} H_x\,,$$
$$M_z = \mu_z\tanh\left(\frac{\Delta}{2k_BT}\right) + \chi_z^{VV} H_z\,, \qquad (3)$$

where $\chi_{x,z}^{VV}$ are the Van-Vleck susceptibilities of rare earth ions. For Pr^{3+} we have $\mu_x = 2.1\ \mu_B$, $\mu_z = 0$ and $\chi_{x,z}^{VV}$ = = $0.15\cdot10^{-4}$ emu/f.u. [6].

Therefore we can write the spatially averaged total magnetic moment $M_{\text{Pr–Mn}}$ of Pr–Mn system:

$$M_{\text{Pr–Mn}} = \frac{1}{3}\left(2M_x + M_z\right). \qquad (4)$$

The calculation results of magnetic moment of Mn^{3+} in $PrMnO_3$ in applied magnetic field without contribution (4) are presented in Fig. 2(c). From Fig. 2(c) it is easy to find that the magnetic moments of Mn^{3+} are 1.4, 1.8 and 2.1 for nano-800 °C, nano-900 °C and polysamples, respectively.

Using Eq. (2) for the Nd^{3+} Kramers ion, when the splitting of ground doublet is caused by superexchange between Mn and Nd ions only, one can write the next expression for splitting Δ_i:

$$\Delta_i = 2\left[\Delta_z^2 + \left(\mu_i H_i\right)^2\right]^{1/2}, \qquad (5)$$

where $\Delta_z = 10.1$ K is the splitting by Mn–Nd exchange, $\mu_z = 1.9\ \mu_B$, $\mu_x = 1.8\ \mu_B$ and $\mu_y = 1.2\ \mu_B$ [4]. Substituting (5) in (3) with account for isotropic magnetic moment

$$M_{\text{Nd–Mn}} = \frac{1}{3}\left(M_x + M_y + M_z\right),$$

we obtain the magnetic moment values of Mn ion equal to 1.7, 1.8, 1.9 and 2 μ_B for nano-800 °C, 850 °C, 900 °C and polysamples, respectively. A decrease of magnetic moment of Mn ion with decreasing grain size indicates the weakening of magnetic interactions in nanosamples.

5. Summary

The detailed magnetic and x-ray diffraction investigations of the $PrMnO_3$ and $NdMnO_3$ manganites have allowed to study and to clarify interesting aspects related to the grain size effect on their structural and magnetic properties.

The $REMnO_3$ (RE = Pr, Nd) samples prepared at temperatures below 900 °C using the sol-gel method had the grains corresponding to the nanoparticles, while the powder synthesized at temperatures of 1150–1170 °C was the large-grain (> 240 nm) sample. The grain sizes determined from the x-ray data decrease with decreasing the annealing temperature. The samples investigated had the orthorhombic crystal structure, in which the lattice parameters depend on the grain sizes.

Magnetic data obtained demonstrate the difference between magnetic ordering of poly- and nanopowdered samples. The nanosamples are characterized by smaller value of both the Néel temperature and the paramagnetic Curie temperature that indicates decrease of magnetic interactions in the nanoparticle samples. The values of magnetic moments obtained from the magnetization measurements decrease as the grain size is decreased.

The temperature-dependent $\chi'_{ac}(T)$ and $\chi''_{ac}(T)$ magnetic susceptibilities show a sharp high-temperature peak connected with Mn magnetic moments ordering. The low-temperature maximum is proposed to be due to the polarization of the rare-earth sublattice by an effective exchange field of the Mn ordered sublattice. The ac susceptibility data for poly- and nanosamples demonstrate the strong frequency dependence of $\chi_{ac}(T)$ susceptibility, that indicates the relaxation process near the critical temperatures.

Acknowledgments

The macroscopic magnetic measurements was carried out with the equipment purchased thanks to the financial support of the European Regional Development Fund in the framework of the Polish Innovation Economy Operational Program (contract No. POIG.02.01.00-12-023/08).

1. E. Dagotto, *Nanoscale Phase Separation and Colossal Magnetoresistance*, Springer-Verlag, Berlin (2001).
2. A. Muñoz, J.A. Alonso, M.J. Martinez-Lopez, and M.T. Fernandez-Diaz, *Solid State Commun*. **113**, 227 (2000).
3. A. Muñoz, J.A. Alonso, M.J. Martinez-Lopez, and M.T. Fernandez-Diaz, *J. Phys.: Condens. Matter* **12**, 1361 (2000).
4. J. Hemberger, M. Brando, R. When, V.Yu. Ivanov, A.A. Mukhin, A.N. Balbashov, and A. Loidl, *Phys. Rev. B* **69**, 064418 (2004).
5. K. Berggold, J. Baier, D. Meier, J.A. Mydosh, T. Lorenz, J. Hemberger, A. Balbashov, N. Aliouane, and D.N. Argyriou, *Phys. Rev. B* **76**, 094418 (2007).
6. A.A. Mukhin, V.Yu. Ivanov, V.D. Travkin, and A.M. Balbashov, *J. Magn. Magn. Mater*. **226–230**, 1139 (2001).
7. V. Dyakonov, F. Bukhanko, V. Kamenev, E. Zubov, S. Baran, T. Jaworska-Gołąb, A. Szytuła, E. Wawrzyńska, B. Penc, R. Duraj, N. Stüsser, M. Arciszewska, W. Dobrowolski, K. Dyakonov, J. Pientosa, O. Manus, A. Nabiałek, P. Aleshkevych, R. Puzniak, A. Wiśniewski, R. Zuberek, and H. Szymczak, *Phys. Rev. B* **74**, 024418 (2006).
8. V. Dyakonov, F.N. Bukhanko, V. Kamenev, E. Zubov, M. Arciszewska, W. Dobrowolski, V. Mikhaylov, R. Puzniak, A. Wiśniewski, K. Piotrowski, V. Varyukhin, H. Szymczak, A. Szytuła, R. Duraj, N. Stüsser, A. Arulraj, S. Baran, B. Penc, and T. Jaworska-Gołąb, *Phys. Rev. B* **77**, 214428 (2008).
9. J. Rodriguez-Carvajal, *Physica B: Condens. Matter* **192**, 55 (1993).
10. B.D. Cullity, *Elements of X-ray Diffraction*, Adison-Wesley, Reading (1978).
11. S.D. Rasberry, *Burean of Standards Certificate — Standard Reference Material* 640b (1987).